INTERNATIONAL JOURNAL FOR NUMERICAL METHODS IN FLUIDS
Int. J. Numer. Meth. Fluids 2007; **54**:73–101
Published online 21 November 2006 in Wiley InterScience (www.interscience.wiley.com). DOI: 10.1002/fld.1394

Direct 2D simulation of small gas bubble clusters: From the expansion step to the equilibrium state

J. Bruchon[1], A. Fortin[1,*,†], M. Bousmina[2] and K. Benmoussa[1]

[1]*GIREF, Département de Mathématiques et de Statistique, Université Laval, Québec, Canada G1K 7P4*
[2]*Département de Génie Chimique, Université Laval, Québec, Canada G1K 7P4*

SUMMARY

A numerical strategy, based on an adaptive finite element method, is proposed for the direct two-dimensional simulation of the expansion of small clusters of gas bubbles within a Newtonian liquid matrix. The velocity and pressure fields in the liquid are first defined through the Stokes equations and are subsequently extended to the gas bubbles. The liquid–gas coupling is imposed through the stress exerted on the liquid by gas pressure (ruled by an ideal gas law) and by surface tension. A level set method, combined with a mesh adaptation technique, is used to track liquid–gas interfaces. Many numerical simulations are presented. The single bubble case allows to compare the simulations to an analytical model. Simulations of the expansion of small clusters are then presented showing the interaction and evolution of the gas bubbles to an equilibrium state, involving topological rearrangements induced by Plateau's rule. Copyright © 2006 John Wiley & Sons, Ltd.

Received 27 February 2006; Revised 28 September 2006; Accepted 30 September 2006

KEY WORDS: level set method; mesh adaptation method; liquid–gas coupling; gas bubble cluster expansion; Laplace's rule; Plateau's rule

1. INTRODUCTION

The study of gas bubbles embedded into a liquid matrix is of great theoretical and industrial interest, at the crossroads of engineering, physics and mathematics [1, 2]. The equilibrium configuration of a bubble cluster is governed by surface tension through two laws: Laplace's law, which relates the curvature of the interface to the pressure difference inside and outside; Plateau's rule, which states that bubbles can meet only in groups of three, at angles of 120°. This last rule

*Correspondence to: A. Fortin, GIREF, Département de Mathématiques et de Statistique, Université Laval, Québec, Canada G1K 7P4.
†E-mail: afortin@giref.ulaval.ca

Contract/grant sponsor: NSERC

implies a minimal surface area property, leading to instabilities and topological rearrangements into larger clusters. In the literature, such situations are investigated in the framework of liquid foams (see [3–5]). Usual approaches for modelling and simulating these phenomena are essentially based on minimal surface area criteria (see [6, 7]).

The present paper proposes a direct simulation, using a finite element method, of the evolution of a set of bubbles into a Newtonian fluid. The first difficulty of this approach is the liquid–gas coupling: the gas is a compressible fluid, having an inner pressure ruled by the ideal gas law, and exerting a stress on the liquid matrix. When the pressure is not balanced by surface tension forces (equilibrium is not yet reached), this stress allows for the expansion of the gas (see [8]). The second difficulty is to obtain a good description of the interfaces: bubbles interact between themselves and can adopt a wide variety of shapes. Furthermore, the interfaces come very close to each other during the process. Consequently, if the numerical method is not accurate enough, numerical diffusion can provoke a purely artificial (numerical) coalescence of bubbles (see Fortin and Benmoussa [9]). The interface tracking method used in the present work is the level set method coupled with an adaptive remeshing strategy which is more completely described by Fortin and Benmoussa [10].

Section 2 of this paper is devoted to the mathematical description of the expansion of a bubble cluster into a liquid matrix, and to its finite element discretization. In Section 3, the expansion of a single bubble is studied. The simulations are compared with an analytical model when neglecting surface tension, and to the Laplace's law otherwise. Section 4 investigates the expansion of several bubbles: cases with three, four and nine bubbles allow for the comparison between simulations and real cluster configurations.

2. MATHEMATICAL FORMULATION

Let us consider a computational domain Ω, a square of $\mathbb{R}^2$, filled with a gaseous part Ω_g embedded into a Newtonian liquid matrix Ω_m (see Figure 1). The gas and the liquid are assumed to be immiscible. At the liquid–gas interface, the gas exerts a stress $(\gamma\kappa - p_g)\mathbf{n}$ on the liquid part, where p_g is the gas pressure (Pa), γ is the surface tension coefficient (N/m), κ is the local curvature (1/m) and $\mathbf{n}$ the unit normal to the interface. Under this gas stress, the liquid flows through the boundary of Ω. Consequently, the gas expands and its volume increases while its pressure, which is governed by an ideal gas law, decreases. The equilibrium state is reached when $p_g - p_{ext} = \gamma\kappa$ (Laplace's law), where p_{ext} is the macroscopic stress imposed over $\partial\Omega$.

The gaseous domain Ω_g is assumed to be a set of n distinct bubbles $\Omega_{g_i} : \Omega_g = \bigcup_{i=1}^{n} \Omega_{g_i}$. For the moment, the location of each domain Ω_m and Ω_{g_i} is assumed to be known over time. The numerical strategy used to track these domains is based on a level set method, which allows an excellent description of moving interfaces. The method requires the whole computational domain being meshed (not only Ω_m) and the problem must therefore be formulated over all Ω. For this reason, the velocity and the pressure fields $\mathbf{v}$ and p must be defined over Ω. Equations governing these fields are first established in the liquid matrix and then extended to the gaseous domain.

2.1. Conservation and equilibrium equations in the liquid domain

In this work, the liquid matrix is assumed to be an incompressible Newtonian fluid in order to focus only on surface tension effects and on liquid–gas coupling. The described numerical method

DOI: 10.1002/fld

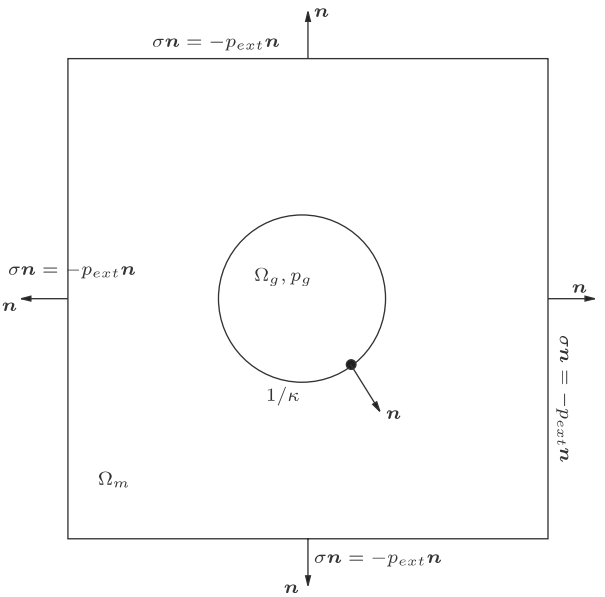

Figure 1. Expansion of a gas bubble into a liquid matrix.

is however general and has been implemented in order to work equally well with shear-thinning fluids governed by power or Carreau laws relating the liquid viscosity to the norm of the strain rate tensor.

The Cauchy stress tensor σ in the fluid matrix is defined by $\sigma = 2\eta_{\mathrm{m}}\varepsilon(\mathbf{v}) - pI$, where η_{m} is the matrix viscosity. Influence of inertia can be evaluated through the Reynolds number Re, which is obtained by balancing inertia and the viscosity terms in the momentum equation. Everitt *et al.* [11] proposed the following definition for foam systems:

$$Re = \frac{\rho V_0^{2/3}(p_{\mathrm{g}}^0 - p_{\mathrm{ext}})}{\eta_{\mathrm{m}}^2} \tag{1}$$

where ρ is the matrix density, V_0 the initial bubble volume and p_{g}^0 the initial gas pressure. This value is generally very small in typical real 2D foam systems (see also Kern *et al.* [12]). Consequently, momentum and mass conservation laws lead to the Stokes equations governing $\mathbf{v}$ and p:

$$\begin{aligned}
&\nabla \cdot [2\eta_{\mathrm{m}}\varepsilon(\mathbf{v})] - \nabla p = 0 && \text{in } \Omega_{\mathrm{m}} \\
&\nabla \cdot \mathbf{v} = 0 && \text{in } \Omega_{\mathrm{m}} \\
&\sigma\mathbf{n} = (\gamma\kappa I + \sigma_{\mathrm{g}_i})\mathbf{n} && \text{on } \partial\Omega_{\mathrm{m}} \cap \partial\Omega_{\mathrm{g}_i} \\
&\sigma\mathbf{n} = -p_{\mathrm{ext}}\mathbf{n} && \text{on } \partial\Omega_{\mathrm{m}} \cap \partial\Omega
\end{aligned} \tag{2}$$

where σ_{g_i} is the Cauchy stress tensor of the ith gas bubble.

DOI: 10.1002/fld

2.2. Conservation and equilibrium equations in a gas bubble

The pressure p_{g_i} in the bubble Ω_{g_i} and its volume $|\Omega_{g_i}|$ are governed by an ideal gas law which, at constant temperature, gives:

$$p_{g_i}|\Omega_{g_i}| = \text{constant}_i \tag{3}$$

In this quasi-static model, the gas pressure is uniform in each bubble. Equation (3) does not allow to describe the velocity field in the gas. However, the evolution of the volume of a bubble depends only on the interface velocity. Hence, the velocity field already defined in Ω_m, is extended to Ω_g in such a way that it does not perturb the interfacial velocity:

$$\begin{aligned} &\mathbf{v} \in C^1(\Omega) \\ &\nabla \cdot [2\eta_g \varepsilon(\mathbf{v})] = 0 \quad \text{in } \Omega_g \end{aligned} \tag{4}$$

where η_g is a (small) numerical parameter. Such an extension corresponds to the addition of a viscosity term to the gas bubble Cauchy stress tensor: $\sigma_{g_i} = 2\eta_g \varepsilon(\mathbf{v}) - p_{g_i} I$. In order to ensure the consistency of the model, the parameter η_g must be chosen small enough so that,

$$2\eta_g \|\varepsilon(\mathbf{v})\mathbf{n}\|_{\mathbb{R}^2} \ll p_{g_i} \|\mathbf{n}\|_{\mathbb{R}^2} = p_{g_i} \tag{5}$$

on $\partial\Omega_{g_i}$. Finally, the pressure field, already defined in Ω_m, has also to be extended to Ω_{g_i}. A natural extension is to set the pressure field p equal to the gas pressure into each bubble as in Caboussat *et al.* [13]

$$p = p_{g_i} \quad \text{in } \Omega_{g_i} \tag{6}$$

However, the Cauchy stress tensor σ_{g_i} is not related to the pressure field p, but is directly a function of p_{g_i}, the bubble pressure. Hence, the value of p in Ω_{g_i} does not appear in Equations (2), and, consequently, can be chosen arbitrarily. This is why, in order to limit the perturbation of the velocity and pressure fields already defined in Ω_m, p is extended by zero in Ω_g

$$p = 0 \quad \text{in } \Omega_g \tag{7}$$

2.3. Velocity–pressure mixed variational formulation

Let us define the functional spaces $\mathscr{V} = (H^1(\Omega))^2$ and $\mathscr{P} = L^2(\Omega)$. The global mixed formulation is obtained by adding the variational forms of (2), (4) and (7). The weak form of (2) in the liquid domain is straightforward:

$$\begin{aligned} &\int_{\Omega_m} 2\eta_m \varepsilon(\mathbf{v}) : \varepsilon(\mathbf{w}) - \int_{\Omega_m} p \nabla \cdot \mathbf{w} = -\int_{\partial\Omega} p_{ext} \mathbf{n} \cdot \mathbf{w} - \int_{\partial\Omega_g} \gamma\kappa \mathbf{n} \cdot \mathbf{w} - \sum_{i=1}^{n} \int_{\partial\Omega_{g_i}} \sigma_{g_i} \mathbf{n} \cdot \mathbf{w} \\ &\int_{\Omega_m} q \nabla \cdot \mathbf{v} = 0 \end{aligned} \tag{8}$$

DOI: 10.1002/fld

$\forall(\mathbf{w}, q) \in \mathscr{V} \times \mathscr{P}$. A similar formulation can be obtained in the gaseous part of the domain from Equations (4) and (7)

$$\begin{aligned} \int_{\Omega_g} 2\eta_g \varepsilon(\mathbf{v}) : \varepsilon(\mathbf{w}) &= \sum_{i=1}^{n} \int_{\partial\Omega_{g_i}} (\sigma_{g_i}\mathbf{n} + p_{g_i}\mathbf{n}) \cdot \mathbf{w} \\ \int_{\Omega_g} pq &= 0 \end{aligned} \tag{9}$$

$\forall(\mathbf{w}, q) \in \mathscr{V} \times \mathscr{P}$. In order to avoid dealing with surface integrals, these latter have to be turned into volume integrals. The divergence theorem can directly be applied to the surface integral involving the gas pressure. The surface tension term can be rewritten as a volumetric force as in Brackbill *et al.* [14] and Béliveau *et al.* [15]. Assuming the interface $\partial\Omega_g$ is smooth enough, the following relation takes place in a distributional sense:

$$\nabla F = \mathbf{n}\delta_{\partial\Omega_g} \tag{10}$$

where $\delta_{\partial\Omega_g}$ is the Dirac distribution associated with $\partial\Omega_g$ and F, the characteristic function of Ω_g, is equal to 1 in Ω_g and vanishes in Ω_m. Relation (10) allows writing

$$\int_{\partial\Omega_g} \gamma\kappa\mathbf{n} \cdot \mathbf{w} = \int_{\Omega} \gamma\kappa\nabla F \cdot \mathbf{w} \tag{11}$$

To avoid the explicit computation of the local curvature κ, the following equality, proved in [15] is considered:

$$\int_{\Omega} \gamma\kappa\nabla F \cdot \mathbf{w} = \int_{\Omega} \gamma \left(\frac{\nabla F \otimes \nabla F - |\nabla F|^2 I}{|\nabla F|} \right) : \nabla\mathbf{w} =: \int_{\Omega} \gamma\mathbf{T} : \nabla\mathbf{w} \tag{12}$$

The second-order tensor $\gamma\mathbf{T}$ will impose surface tension forces at the boundary of each gas bubble. By adding systems (8) and (9) and by taking into account relations (11) and (12), the final mixed system is:

Find $(\mathbf{v}, p) \in \mathscr{V} \times \mathscr{P}$ such that

$$\begin{aligned} &\int_{\Omega_m} 2\eta_m \varepsilon(\mathbf{v}) : \varepsilon(\mathbf{w}) + \int_{\Omega_g} 2\eta_g \varepsilon(\mathbf{v}) : \varepsilon(\mathbf{w}) - \int_{\Omega_m} p\nabla \cdot \mathbf{w} \\ &\quad = -\int_{\partial\Omega} p_{ext}\mathbf{w} \cdot \mathbf{n} - \int_{\Omega} \gamma\mathbf{T} : \nabla\mathbf{w} + \int_{\Omega} p_g \nabla \cdot \mathbf{w} \\ &\quad\quad - \int_{\Omega_m} q\nabla \cdot \mathbf{v} - \alpha_p \int_{\Omega_g} p\, q = 0 \quad \forall(\mathbf{w}, q) \in \mathscr{V} \times \mathscr{P} \end{aligned} \tag{13}$$

where the gas pressure p_g equals p_{g_i} in Ω_{g_i} and vanishes in the liquid matrix Ω_m and α_p is a numerical parameter, which allows to add the last equations of systems (8) and (9), and has the dimensions of the inverse of a viscosity. In the continuous case (13), $\Omega_m \cap \Omega_g = \emptyset$ and the parameter α_p is then arbitrary. However, in the discrete case, for a same given node, the contributions to the mass matrix can be provided by both liquid and gaseous terms and α_p appears therefore as

DOI: 10.1002/fld

a weighting parameter. More precisely, it has to be chosen small enough to ensure mass conservation in the liquid domain ($\alpha_p = 10^{-5}$ in the presented simulations).

Before discussing the finite element implementation used for solving system (13), some important points have to be outlined:

- The uniqueness of the solution of (13) is ensured by considering Dirichlet conditions for the velocity $\mathbf{v}$ over a part of the boundary $\partial\Omega$. These conditions will be defined in the following for each considered case.
- The gas pressure field involved in (13) is calculated with n relations of the form (3). The simulations require the volume of each bubble, and need a special treatment (see Section 4).
- By construction, the velocity and the pressure fields ($\mathbf{v}$, p) solution of (2), (4) and (7), are also a solution of the weak mixed formulation (13). In turn, if $\mathbf{v}$ and p are solutions of (13), and if the gas boundary is smooth enough, then $\mathbf{v}$ and p are also solutions of (2), (4) and (7) (in a distributional sense) and satisfy the boundary and interface conditions considered in (2).

In order to use a finite element method for solving system (13), the integrals defined over Ω_m and Ω_{g_i} have to be turned into integrals defined over Ω. Such an operation is performed by considering the characteristic function F of the gaseous domain, and its complementary function $1 - F$. Multiplying the integrand by F (or $(1 - F)$) will restrict the integral to Ω_g (or Ω_m):

$$\int_{\Omega_g} f \, d\Omega = \int_{\Omega} F f \, d\Omega, \quad \int_{\Omega_m} f \, d\Omega = \int_{\Omega} (1 - F) f \, d\Omega$$

The second-order ($O(h^2)$) Taylor–Hood finite element (quadratic velocity and linear pressure) is then used to discretize the resulting mixed formulation. Finally, the finite element implementation is achieved by computing the characteristic function F of the gaseous part i.e. by computing the evolution of the bubble position over time.

2.4. Interface capturing

The methodology used to capture the interfaces is described in detail in [10] and is based on a finite element approach and a level set method. Let us consider a function $\phi : \Omega \times \mathbb{R}^+ \to \mathbb{R}$ describing the gaseous domain Ω_g. Since Ω_g is convected by the velocity field $\mathbf{v}$, ϕ is solution of a pure advection equation [16]

$$\begin{aligned} &\frac{\partial \phi}{\partial t} + \mathbf{v} \cdot \nabla \phi = 0 \quad \forall t > 0 \\ &\phi(.\,, 0) = \phi_0 \qquad \text{at } t = 0 \end{aligned} \tag{14}$$

Solving such a hyperbolic equation is a difficult numerical task [17], and may involve spurious oscillations when using standard finite elements. The level set method, developed in [16], avoids the development of steep gradients by convecting a smooth function ϕ. More precisely, ϕ is the signed distance function to the interface $\partial\Omega_g$, which is positive for Ω_g, vanishes over $\partial\Omega_g$ and is negative for Ω_m. Using this approach, $\phi \in \mathscr{C}^1(\Omega)$ and $\|\nabla\phi\|_{\mathbb{R}^2} = 1$. Equation (14) can then be solved by a classical SUPG method.

DOI: 10.1002/fld

As in [10], the simulations presented in this paper have been performed by using such a level set method, with quadratic polynomials for the space discretization of ϕ and an implicit Euler scheme for the time derivative. Note that even though ϕ_0 is initially a signed distance function, the solution ϕ of Equation (14) does not generally conserve this property. Hence, steep gradients may progressively appear near the interface which becomes irregular. Consequently, after solving Equation (14), an additional re-initialization step is necessary, which consists in modifying the solution for obtaining $\|\nabla\phi\|_{\mathbb{R}^2} = 1$, without changing the isovalue zero, i.e. without perturbing the interface position (see Sussman and Fatemi [18]).

When solving a hyperbolic equation like (14), boundary conditions have to be imposed only over the inflow part of the boundary $\partial\Omega$. Since the velocity field $\mathbf{v}$ involved in (14) is the expansion velocity field, solution of (13), $\partial\Omega$ is usually an outflow boundary. Consequently, function ϕ does not verify any boundary condition.

In the discrete case, the gas characteristic function F has to be smoothed out and is thus defined by the following:

$$F = \begin{cases} 0 & \text{if } \phi \geqslant \varepsilon \\ \dfrac{1}{2}\left(1 - \dfrac{\phi}{\varepsilon} - \dfrac{1}{\pi}\sin\left(\pi\dfrac{\phi}{\varepsilon}\right)\right) & \text{if } |\phi| \leqslant \varepsilon \\ 1 & \text{if } \phi \leqslant -\varepsilon \end{cases} \tag{15}$$

where ε is a regularization parameter. Hence, the effective computed interface has a width of 2ε. This smooth form of F allows to consider its gradient, which is used to express the surface tension tensor T in relation (12): $\nabla F = (\mathrm{d}F/\mathrm{d}\phi)\nabla\phi$.

To improve the accuracy on the interface location, a mesh adaptation method is used (see [19, 20]). This method is based on a hierarchical error estimator. It concentrates the mesh elements in the vicinity of the interfaces and allows to choose very small values of ε and thus very thin interfaces. Hence, a good description of the interfaces is obtained with an acceptable number of mesh elements.

2.5. Units used in the simulations

Simulation results considered here are given in a dimensionless form. More precisely, let $\overline{x}$ be the characteristic length of the computational domain, and let $\overline{p}$ be the characteristic pressure. The corresponding characteristic time is $\overline{t} = \eta_{\mathrm{m}}/\overline{p}$, the characteristic velocity is defined by $\overline{v} = \overline{x}/\overline{t}$.

Let us consider the following decompositions: $x = x^*\overline{x}$, $y = y^*\overline{y}$, $t = t^*\overline{t}$, $p = p^*\overline{p}$, $v = v^*\overline{v}$, $\gamma = \gamma^*\overline{p} \times \overline{x}$ where x^*, y^*, t^*, p^*, v^* and γ^* are dimensionless numbers. For instance, by considering $\eta_{\mathrm{m}} = 1$ Pa/s, $\overline{x} = 10^{-2}$ m and $\overline{p} = 10^2$ Pa, then $\overline{t} = 10^{-2}$ s, $\overline{v} = 1$ m/s and $\overline{\gamma} = 1$ N/m.

System (13) has been solved by using the dimensionless quantities. Hence, whatever the physical quantity q considered here, it is always its dimensionless part q^* which is given. The physical value of q is then equal to $q^*\overline{q}$.

3. DIRECT SIMULATION OF SINGLE BUBBLE EXPANSION

In this rather simple case, an analytical model is developed for the expansion of a single bubble. This model provides an analytical expression for the radius of a circular gas bubble growing into an

DOI: 10.1002/fld

infinite Newtonian matrix, when neglecting surface tension. Comparisons between this theoretical model and our simulation will thus be possible allowing to test the efficiency of the presented approach. Surface tension will then be introduced and its effect on the expansion will be tested.

3.1. Analytical model

Let us consider the growth of a disk of radius $R(t)$, within an infinite matrix of a Newtonian liquid. Cylindrical co-ordinates (r, θ) are used with the origin O chosen at the bubble centre. The kinematics of the liquid matrix are ideally described by a purely radial velocity field which depends, as the pressure, only on the r-component: $\mathbf{v} = (u(r), 0),\ p = p(r)$. The initial bubble radius is denoted by $R(0) = R_0$, with a corresponding area V_0 and a bubble pressure p_g^0. The incompressibility condition of the liquid leads to the following:

$$\frac{1}{r}\frac{\mathrm{d}}{\mathrm{d}r}(ru) = 0, \quad r \geqslant R \tag{16}$$

The solution of this first-order differential equation using the condition at the interface $u(R) = \mathrm{d}R/\mathrm{d}t = \dot{R}$ leads to:

$$u(r) = \frac{\dot{R}R}{r}, \quad r \geqslant R \tag{17}$$

Due to the radial symmetry, the momentum balance is described by one single scalar equation

$$\frac{\mathrm{d}\sigma_{rr}}{\mathrm{d}r} + \frac{1}{r}(\sigma_{rr} - \sigma_{\theta\theta}) = 0 \tag{18}$$

which is completed with the following appropriate boundary conditions:

$$\begin{aligned} \sigma_{rr}(R) &= -p_g \\ \sigma_{rr}(+\infty) &= -p_{ext} \end{aligned} \tag{19}$$

Considering expression (17), the strain rate tensor is of the form:

$$\varepsilon(\mathbf{v}) = \frac{\dot{R}R}{r^2}\begin{pmatrix} -1 & 0 \\ 0 & 1 \end{pmatrix} \tag{20}$$

and Equation (18) becomes: $\mathrm{d}p/\mathrm{d}r = 0$. Furthermore, Equations (19) and (20) imply that $p(+\infty) = p_{ext}$. The pressure is thus constant in the liquid

$$p(r) = p_{ext}, \quad r > R \tag{21}$$

Finally, by considering the first condition in Equation (19) and the stress at $r = R$, the growth velocity $\dot{R}$ can be expressed as

$$\frac{\dot{R}}{R} = \frac{p_g - p_{ext}}{2\eta_m} \tag{22}$$

This analytical expression is very useful in order to understand the expansion of a bubble, and the above results require some comments. First, note the absence of shear stress in (20). Second,

DOI: 10.1002/fld

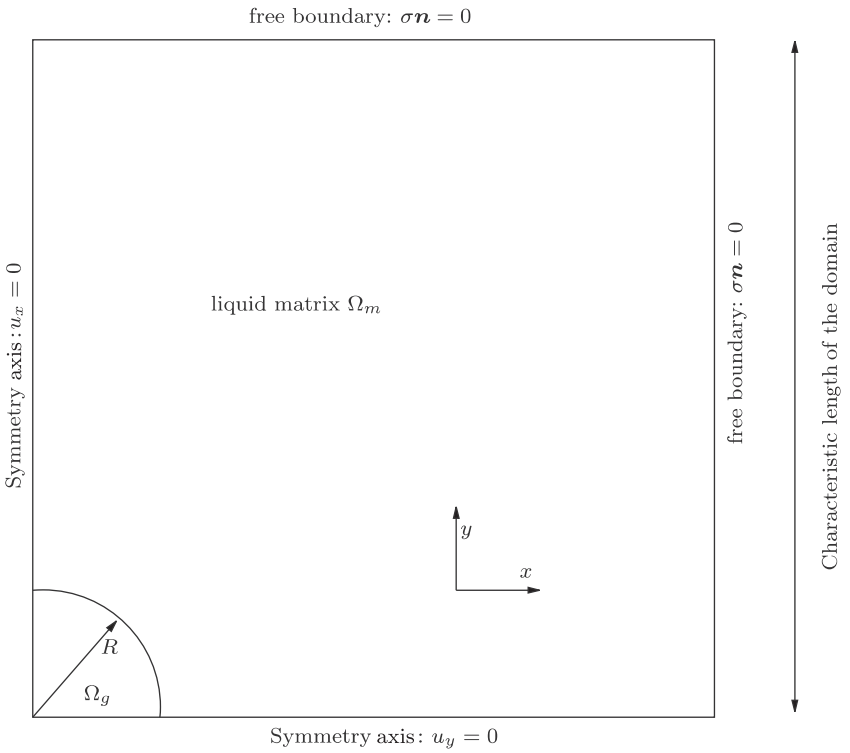

Figure 2. Computational domain for the expansion of a single gas bubble.

since the pressure is constant in the liquid matrix, the liquid–gas interface is a discontinuity surface (or line in 2D) for the pressure but the normal stress is continuous across this surface when surface tension is neglected. Furthermore, the local growth velocity, expressed by Equation (22), depends only on the local pressure difference which also corresponds to the global pressure difference.

In order to solve Equation (22), the gas pressure has to be related to the radius. Three cases can be distinguished:

Constant gas pressure: $p_g(t) = p_g^0$ and

$$R(t) = R_0 \exp\left(\frac{(p_g - p_{ext})t}{2\eta_m}\right) \tag{23}$$

Ideal gas law: $p_g V = p_g^0 V_0$, i.e. $p_g = p_g^0 R_0^2 / R^2$ and if $p_{ext} \neq 0$, then

$$R(t) = R_0 \left[\frac{p_g^0}{p_{ext}} + \left(1 - \frac{p_g^0}{p_{ext}}\right) \exp\left(-\frac{p_{ext} t}{\eta_m}\right)\right]^{1/2} \tag{24}$$

DOI: 10.1002/fld

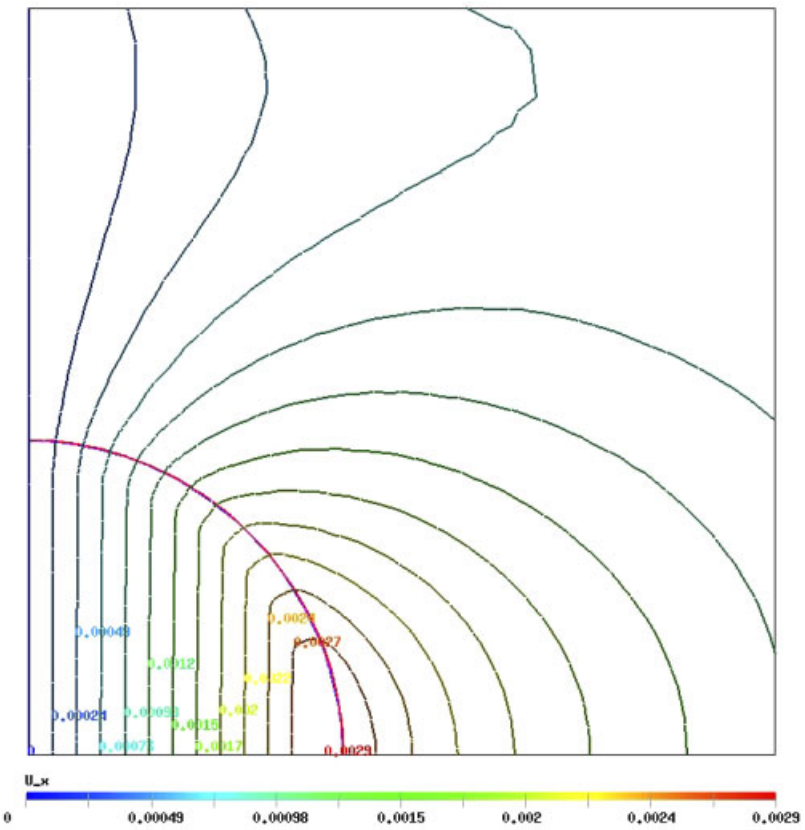

Figure 3. Expansion of a gas bubble: interface and first component of the velocity field.

if $p_{\text{ext}} = 0$, then

$$R(t) = R_0 \left(1 + \frac{p_{\text{g}}^0 t}{\eta_{\text{m}}}\right)^{1/2} \tag{25}$$

3.2. Numerical results without surface tension

The presented simulations of the expansion of a single bubble have been performed in the configuration shown in Figure 2. Symmetry considerations allow for considering only one quarter of the bubble. Appropriate Dirichlet boundary conditions have therefore been imposed over symmetry axes: $v_x = 0$ is enforced on $\{x = 0\}$, and $v_y = 0$ on $\{y = 0\}$, with $\mathbf{v} = (v_x, v_y)$. Surface tension is neglected ($\gamma = 0$) and the ambient pressure p_{ext} is set equal to zero. Hence, the bubble can grow indefinitely. The initial bubble pressure is $p_{\text{g}}^0 = 0.2$, its initial radius is $R_0 = 0.1$, the matrix viscosity η_{m} is equal to 1, and the value of η_{g} is 10^{-3}. These parameters are expressed in the chosen units.

DOI: 10.1002/fld

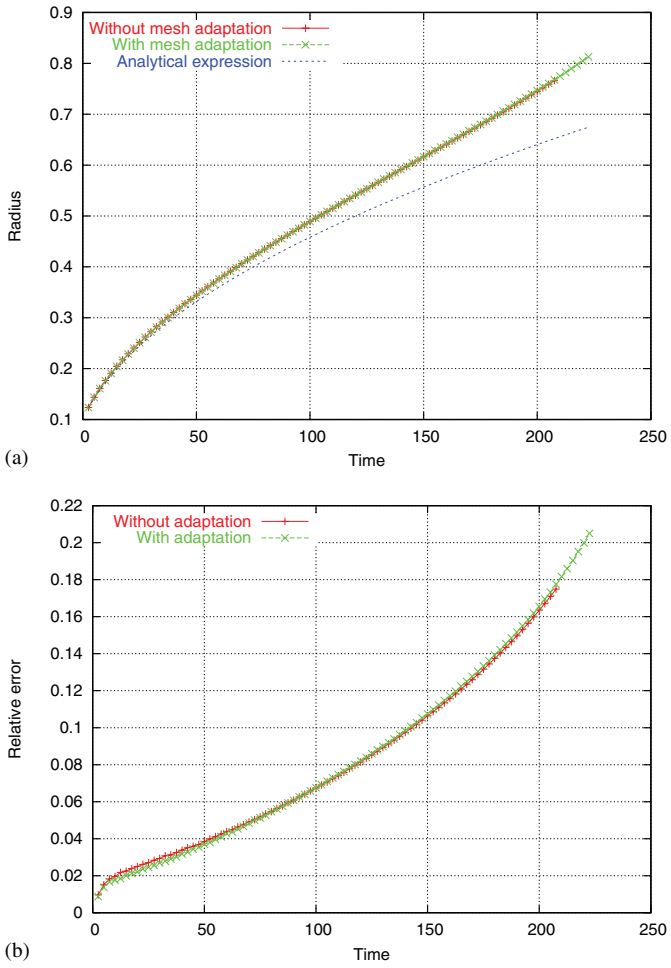

Figure 4. Expansion of a disk of initial radius 0.1 into a domain of length 1: (a) bubble radius: comparison between theory and simulation; and (b) relative error $|R - R_h|/R$.

Regarding the ideal gas law (3), the bubble pressure is defined by: $p_b = p_g^0 V_0/|\Omega_g|$, where

$$|\Omega_g| = \int_{\Omega_g} 1 \, d\Omega = \int_{\{\phi<0\}} 1 \, d\Omega$$

The gas pressure field, involved in the mixed formulation (13), is then defined by: $p_g = p_b F$.

Figure 3 shows the liquid–gas interface superimposed on isovalues of the first component of the computed velocity, at a fixed time. As expected, the obtained velocity field is characteristic of an expansion. It reaches its maximal absolute values over the interface, because of the stress exerted by the gas. Figure 4(a) compares, over time, the radius R_h obtained by simulation with the one calculated with the analytical expression (25). Figure 4(b) quantifies this study by expressing the relative error committed on the radius: $e_h = |R - R_h|/R$. Until $t \simeq 50$, the agreement between

DOI: 10.1002/fld

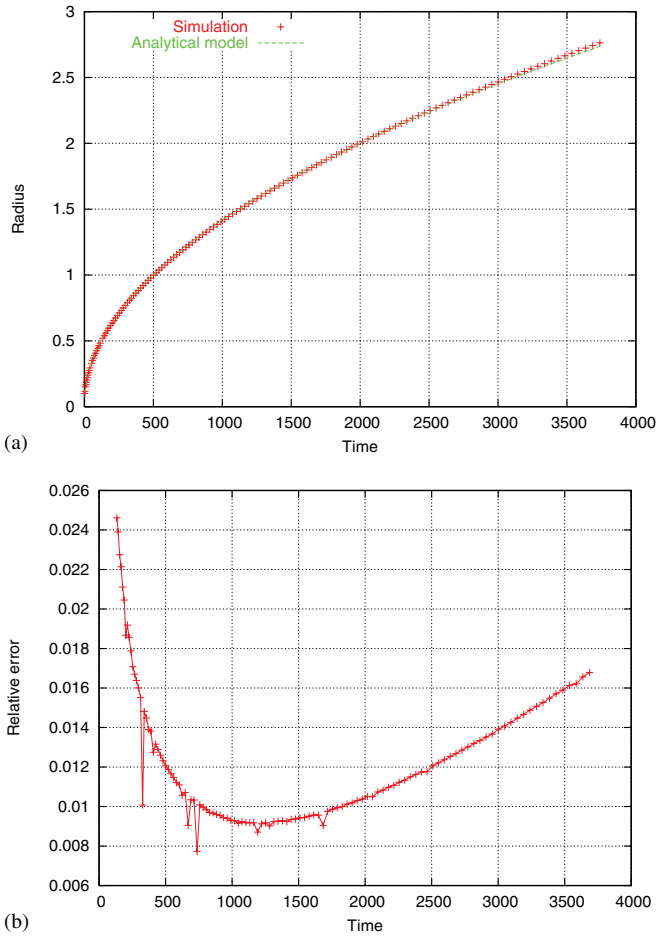

Figure 5. Expansion of a disk of initial radius 0.1 into a domain of length 10: (a) bubble radius: comparison between theory and simulation; and (b) relative error $|R - R_h|/R$.

simulations and theory is quite good, and the relative error is smaller than 4%. Beyond this value, the error growth seems exponential. The change in the error occurs when the bubble radius reaches one-third of the computational domain length (here, Ω is the unit square). These disappointing results are easily explained by boundary effects. Indeed, the analytical model assumes that the expansion is taking place in an infinite domain, while the computational domain is finite. This analysis is validated in Figure 5, which shows that the simulation results obtained by using a computational domain are 10 times larger than before. As long as the radius is smaller than one-third of the computational domain length, the agreement between simulation and theory is excellent.

Finally, Figure 4 shows that mesh adaptation does not perturb the bubble's expansion. The mesh used to perform the simulations without adaptation has more than 20 000 elements, while the different adapted meshes have between 2000 and 5000 elements. Furthermore, simulations

DOI: 10.1002/fld

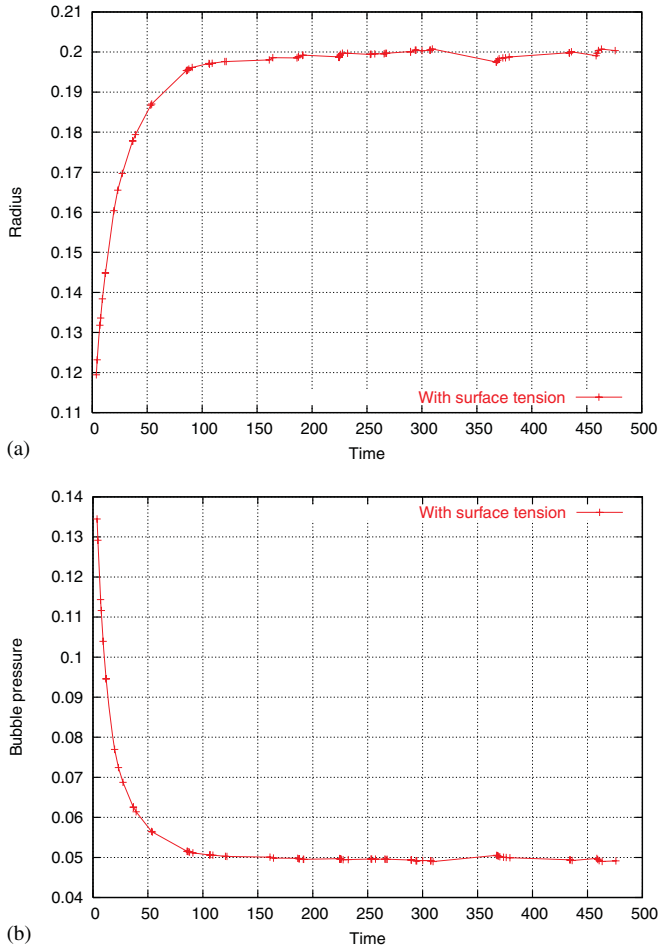

Figure 6. Expansion of a disk of initial radius 0.1 and initial pressure 0.2, into a domain of length 10, with surface tension effect: (a) bubble radius evolution; and (b) bubble pressure evolution.

involving a computational domain having a characteristic length of 10, can be carried out only by using mesh adaptation since the ratio between the computational domain and bubble characteristic lengths is equal to 100 and the number of mesh elements required without mesh adaptation is too high.

3.3. Numerical results with surface tension

Expansion of a single bubble is simulated by considering the same configuration and the same parameters as in Section 3.2, except that surface tension is now taken into account. The surface tension coefficient γ (from Equation (2)) is equal to 10^{-2}. Since p_{ext} is still vanishing, the bubble should grow until the gas pressure p_{b} reaches γ/R. Considering the ideal gas law $p_{\text{b}}R^2 = p_{\text{g}}^0 R_0^2$,

DOI: 10.1002/fld

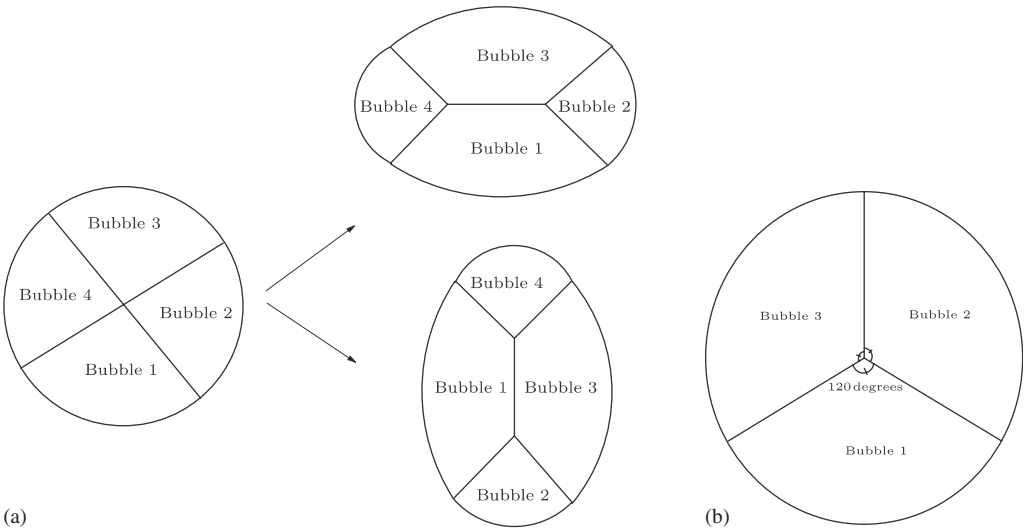

Figure 7. Plateau's rule: (a) topological changes in a four bubble cluster; and (b) three bubbles at an angle of 120°.

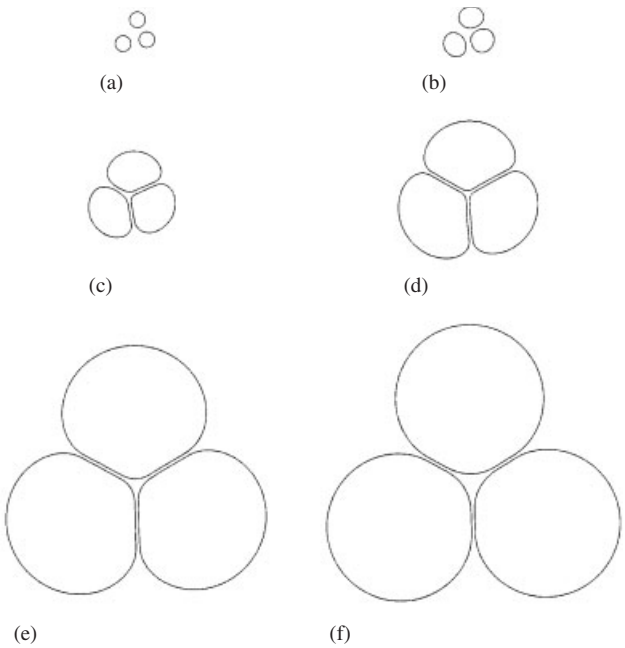

Figure 8. Expansion of three bubbles: (a) $t = 0$; (b) $t = 1.4$; (c) $t = 10$; (d) $t = 37$; (e) $t = 284$; and (f) $t = 824$.

DOI: 10.1002/fld

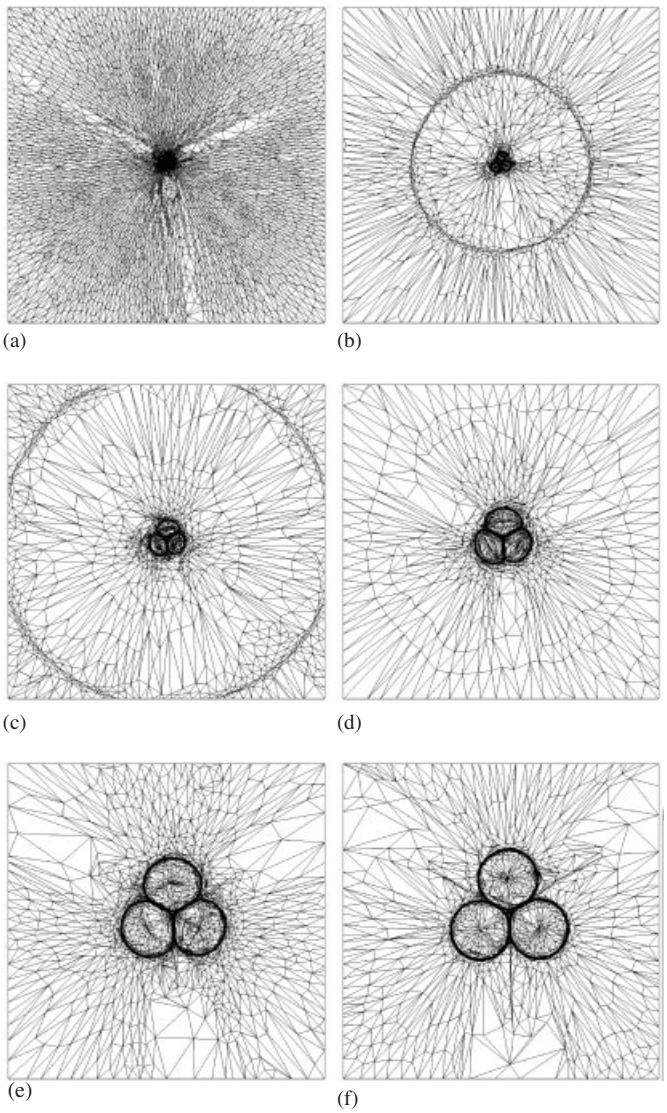

Figure 9. Expansion of three bubbles: meshes: (a) $t = 0$; (b) $t = 1.4$; (c) $t = 10$; (d) $t = 37$; (e) $t = 284$; and (f) $t = 824$.

the corresponding equilibrium radius is

$$R_{\mathrm{eq}} = \frac{p_{\mathrm{g}}^0 R_0^2}{\gamma} \tag{26}$$

Figure 6 presents the results of a simulation performed using a computational domain having a characteristic length of 10. Since $p_{\mathrm{g}}^0 = 0.2$ and $R_0 = 0.1$, the theoretical equilibrium radius is

DOI: 10.1002/fld

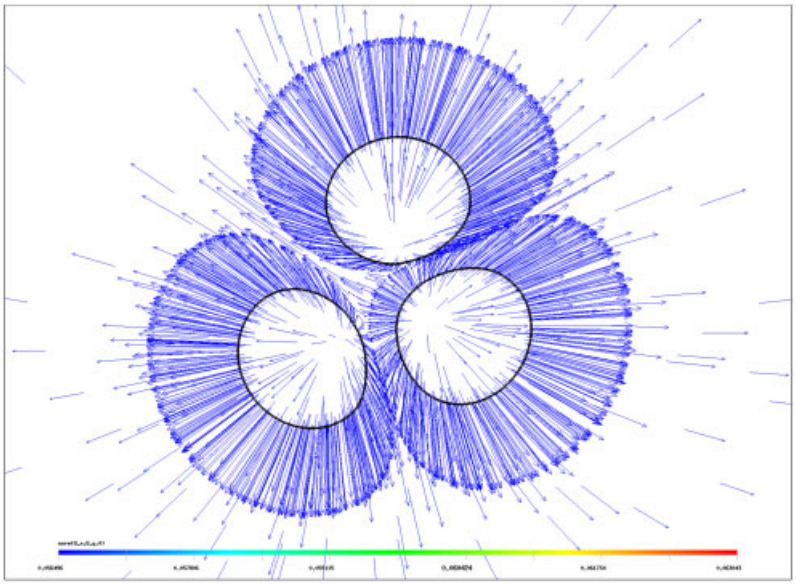

(a)

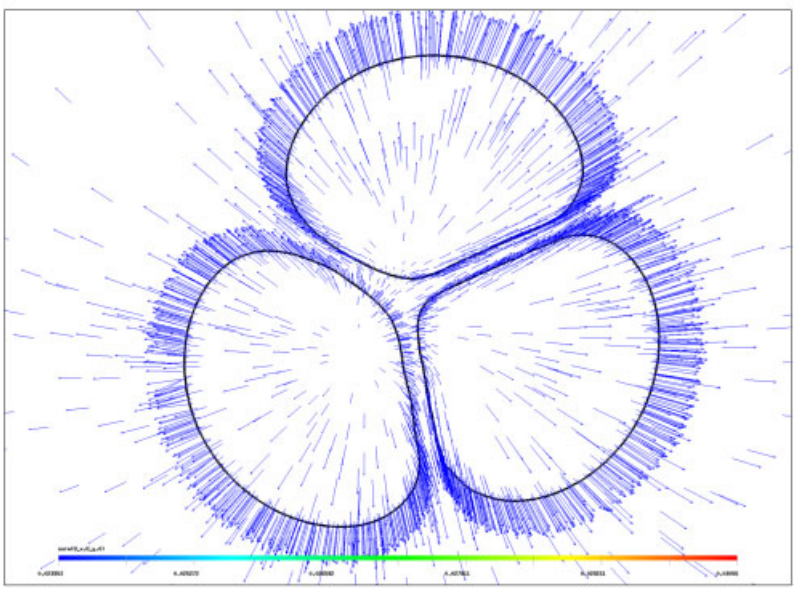

(b)

Figure 10. Expansion of three bubbles: velocity field (first stage of the expansion): (a) $t = 1.4$; and (b) $t = 10$.

DOI: 10.1002/fld

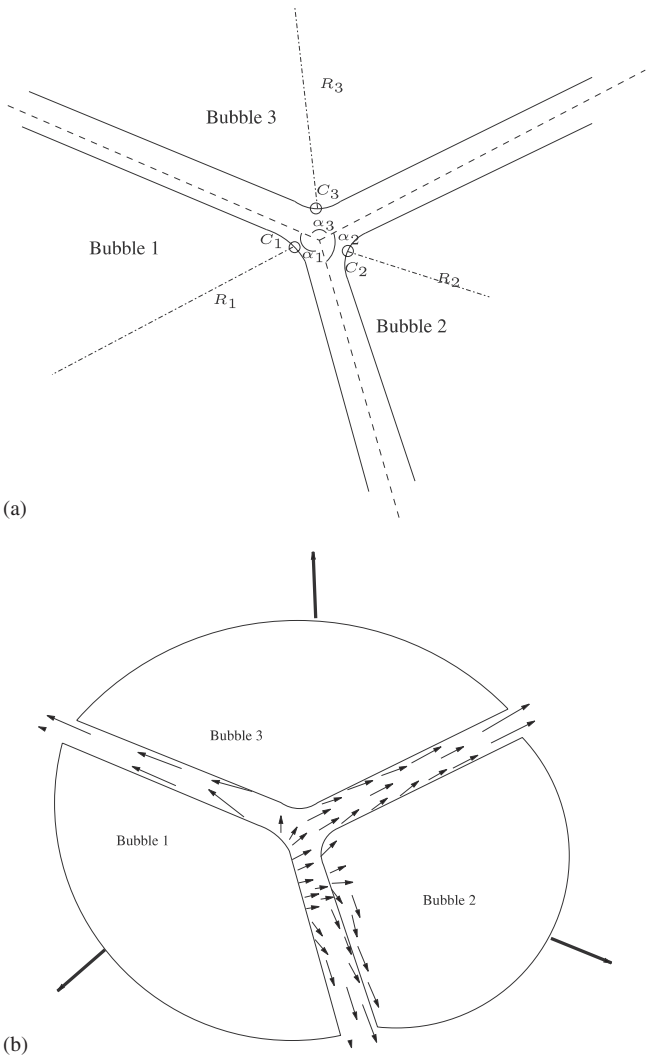

Figure 11. Plateau's rule: three bubbles reaching to their equilibrium state: (a) unstable state; and (b) velocity due to the difference of curvatures.

$R_{\text{eq}} = 0.2$, and the associated equilibrium pressure is $p_{\text{eq}} = 5 \times 10^{-2}$. These equilibrium values are exactly those reached by the simulation. The small oscillations observed in Figure 6 are due to the change in the time step, which increases over time.

4. DIRECT SIMULATION OF THE EXPANSION OF BUBBLE CLUSTERS

The previous simulations, involving only one bubble, have proved the accuracy of the developed method for the liquid–gas coupling. They have also validated the approach for the computation

DOI: 10.1002/fld

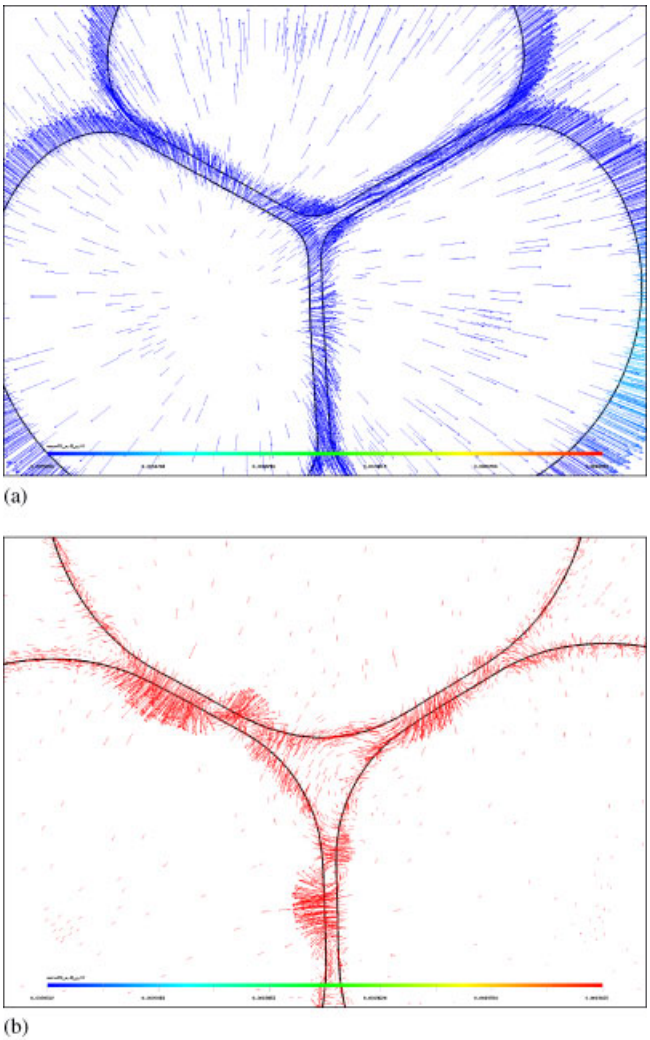

Figure 12. Expansion of three bubbles: velocity field (last two stages of the expansion): (a) $t = 73$; and (b) $t = 670$.

of the surface tension term. Dealing with a bubble cluster adds another degree of complexity to the simulations. The bubbles will now interact between themselves and the corresponding interfaces will get more complicated. Furthermore, due to surface tension effects, the equilibrium configuration of a bubble cluster satisfy both Laplace's law $\gamma\kappa = p_g - p_{ext}$ and Plateau's rule [2]. This last one states, in a liquid foam framework, that bubbles meet in cluster of three, forming angles of 120°. It has to be pointed out that the two different parts composing Plateau's rule are important. Firstly, 'clusters of three' means that the configuration resulting from the meeting of four (or more) bubbles is unstable and leads to topological changes to minimize the interfaces. Such events are depicted in Figure 7(a) for the case involving four bubbles (see [6, 21]). Secondly,

DOI: 10.1002/fld

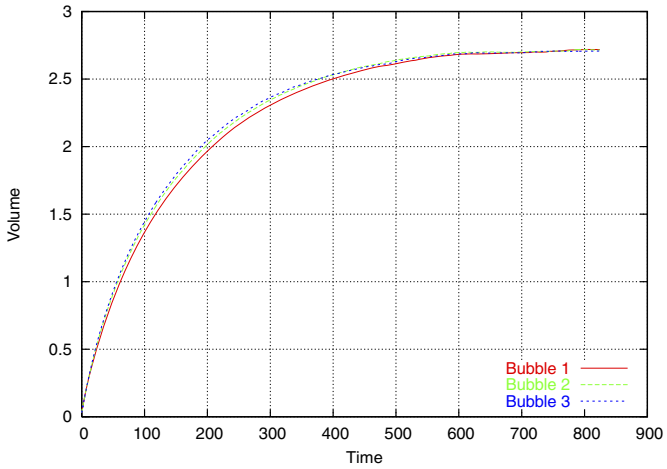

Figure 13. Expansion of three bubbles: evolution of their volumes.

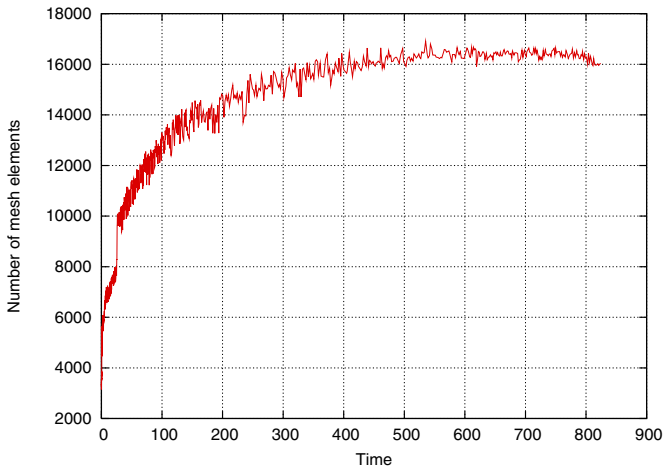

Figure 14. Expansion of three bubbles: evolution of the number of mesh elements.

the resulting angles of 120° (see Figure 7(b)) are a simple consequence of the equilibrium of surface tension forces acting over bubble surfaces. This subject will be detailed in the following.

Since the normal stress p_{ext}, enforced over the boundary of Ω, is constant, the pressure within the liquid domain is constant and equal to p_{ext} (see Section 3.1). Hence, at the equilibrium state, Laplace's law states that for the ith bubble, $p_{g_i} - \gamma/R_i = p_{\text{ext}}$. But p_{g_i} being uniform in the bubble, this relation implies that R_i is uniform and the bubble is spherical (or circular) when reaching its equilibrium state.

To carry out simulations with several bubbles, it is necessary to avoid the 'numerical' coalescence of two neighbouring bubbles which can occur when the mesh is too coarse at the interface between two bubbles. On a coarse mesh, the computation of the signed distance function ϕ giving the

DOI: 10.1002/fld

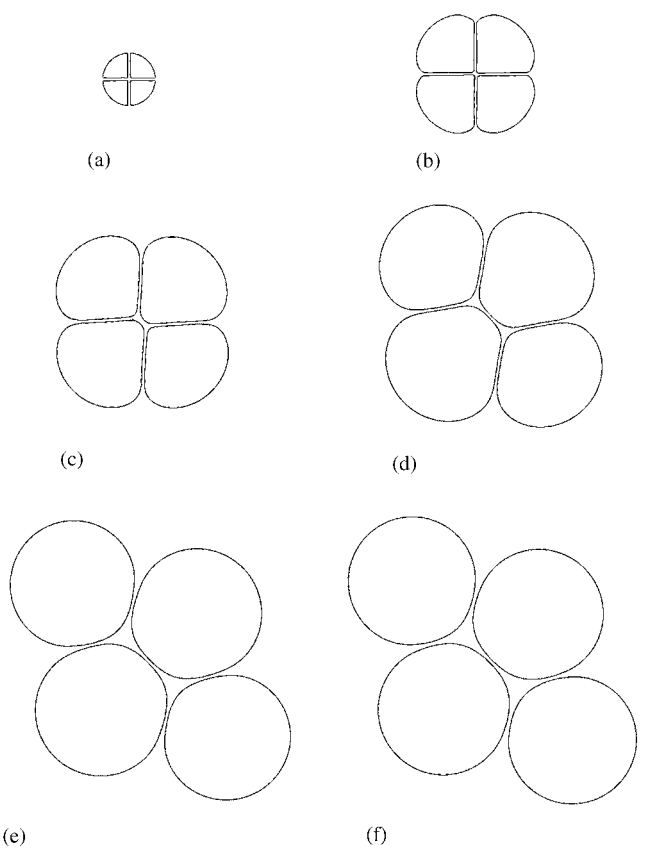

Figure 15. Expansion of four bubbles: (a) $t=0$; (b) $t=7$; (c) $t=23$; (d) $t=59$; (e) $t=225$; and (f) $t=322$.

interfaces position can suffer from excessive numerical diffusion leading to an artificial coalescence of adjacent bubbles. Mesh adaptation plays a major role here. It allows to concentrate the elements in a very narrow band of width 2ε along the interface. In the following computations, ε is set equal to 5×10^{-3}, compared with an initial bubble characteristic length of 0.1.

The computation of the bubble pressures is an another key point of the cluster simulations. From Equation (3), it is necessary to compute the volume of each bubble. If a signed distance function ϕ_i is associated with each bubble Ω_{g_i}, the volume of this bubble is simply given by $|\Omega_{g_i}|=\int_{\phi_i<0}1\mathrm{d}\Omega$. The drawback of this approach is its computational cost since for n bubbles, n distance functions have to be stored and n advection equations have to be solved. To avoid this important cost, one single signed distance function ϕ is considered and an algorithm is developed to rebuild the different bubble volumes.

4.1. Algorithm for bubble volume reconstruction

The liquid–gas coupling exposed in the present paper presents similarities with the one developed by Caboussat *et al.* [13]. The algorithm proposed here is simpler: one single loop over the

DOI: 10.1002/fld

mesh elements is necessary to number all the bubbles and to determine their volumes. In [13], the numbering of the gas bubbles requires the solution of a Poisson equation for each bubble. When the location of a bubble is identified, a loop over the mesh elements enables to compute its volume.

Let EltVisited be a boolean array of length NbElt, the number of elements of the mesh $\mathscr{T}_h(\Omega)$, whose values 0 or 1 correspond to the state of each element: not visited yet or already visited. The aim of the algorithm is to construct BubbleTracker, an integer array, of length NbElt, whose values indicate if an element belongs to the liquid (value 0), or to the ith bubble (value i). Once this array exists, it is very easy to calculate the bubble volumes and the pressure field p_g involved in Equation (13). Hence, $\forall K \in \mathscr{T}_h(\Omega)$, $\forall x \in K$, $p_{g|K}(x) = F_{|K}(x)p_b$, where p_b is the pressure of the bubble number BubbleTracker[K], computed by the ideal gas law (3) (and $p_b = 0$ if BubbleTracker[K] is equal to zero). This approach could be improved by looking for the bubble number at quadrature points. However, the algorithm shows good results without this improvement, which is not considered here. The algorithm is as follows:

```
   begin
integer i ← 0
boolean EltVisited[NbElt]
integer BubbleTracker[NbElt]
while (i < NbElt) {
      EltVisited[i] ← 0   \\ Initialization
      BubbleTracker[i] ← 0
      i ← i + 1
}
Integer NbBubbles ← 0    \\ The number of bubbles
i ← 0
while (i < NbElt) {
      if (EltVisited[i] = = 0) {
            boolean GaseousElt = IsGas(i)
            if (GaseousElt = = 1) {   \\ New bubble
                  NbBubbles ← NbBubbles + 1
                  ExploreNewBubble(i, NbBubbles, EltVisited, BubbleTracker)
             }
             else EltVisited[i] ← 1
      }
      i ← i + 1
}
end
```

The function IsGas(i) evaluates the signed distance function ϕ over the mesh element i and returns the value 1 if $\phi<0$ (the element is in the gas) and the value 0 otherwise. The function ExploreNewBubble(i, NbBubbles, EltVisited, BubbleTracker) explores a new bubble starting from the element i. More precisely, starting from i, this function constructs a new bubble by adding gradually the neighbours of i, the neighbours of the neighbours, and so on, while ϕ is found negative. For each element K added to the bubble, the function sets EltVisited[K] = 1 and BubbleTracker[K] = NbBubbles.

DOI: 10.1002/fld

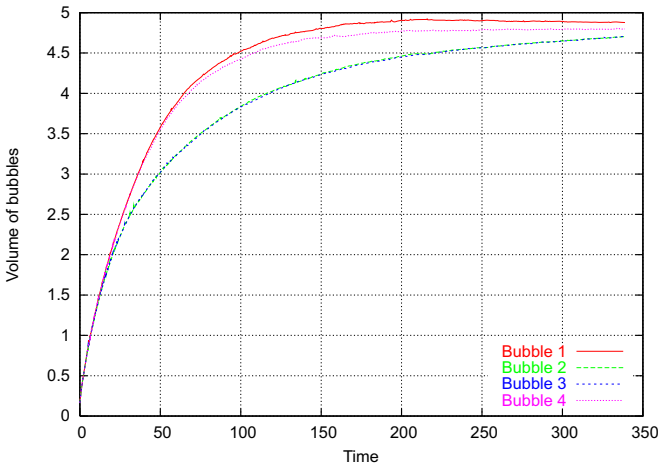

Figure 16. Expansion of four bubbles: evolution of their volumes.

Using this algorithm the number associated with a given bubble can vary from one time step to the next. That is why an additional task is required to determine the number of the ith bubble at the previous time step (and then to know what was its previous volume). Since bubble coalescence or breakup is not allowed, each bubble is simply characterized through the point X located inside this bubble minimizing ϕ. For example, the fact that $X = (x, y) \in \Omega_1$ at the time t_1 and $X \in \Omega_3$ at the time $t_1 + \Delta t$, implies $\Omega_1(t_1) \equiv \Omega_3(t_1 + \Delta t)$, and then

$$p_3(t_1 + \Delta t) = \frac{p_1(t_1)|\Omega_1(t_1)|}{|\Omega_3(t_1 + \Delta t)|}$$

4.2. Expansion of a three bubble cluster

The presented simulation has been carried out by taking $p_{\text{ext}} = 0$, $p^0_{g_i}|\Omega^0_{g_i}| = 0.0314$ and $R^0_i = R^0 = 0.1$, $i = 1, 2, 3$. The surface tension coefficient γ is equal to 10^{-2}. Moreover, the characteristic length of the computational domain is equal to 10. The initial bubble centres are: $(0.15, 0)$, $(-0.15, -0.05)$ and $(0.03, 0.25)$ (see Figure 8(a)). This initial configuration does not respect the angles of 120° between the bubbles. To ensure the uniqueness of the solution of system (13), Dirichlet boundary conditions must be considered: the velocity field is assumed to vanish at the four corners of the squared computational domain. This condition is in agreement with expression (17) of the velocity field: when being far enough from the bubbles, liquid remains at rest. Furthermore, enforcing boundary conditions in the four corners of the domain (and not only in one corner) avoid an additional dissymmetry in the system.

The complete evolution of the bubbles and the corresponding meshes are depicted in Figures 8 and 9. By considering the form of the velocity field (Figures 10 and 12), the expansion of the cluster depicted in Figure 8 can be divided into three different stages. Initially (Figure 8(a)), bubbles have the same uniform curvature, equal to $1/R^0$. During the first stage of the expansion (Figure 8(b)), bubbles interact between themselves, changing their shape and then their local curvature. However, despite this local curvature change, the surface tension term $\gamma\kappa$ has no significant influence on the

DOI: 10.1002/fld

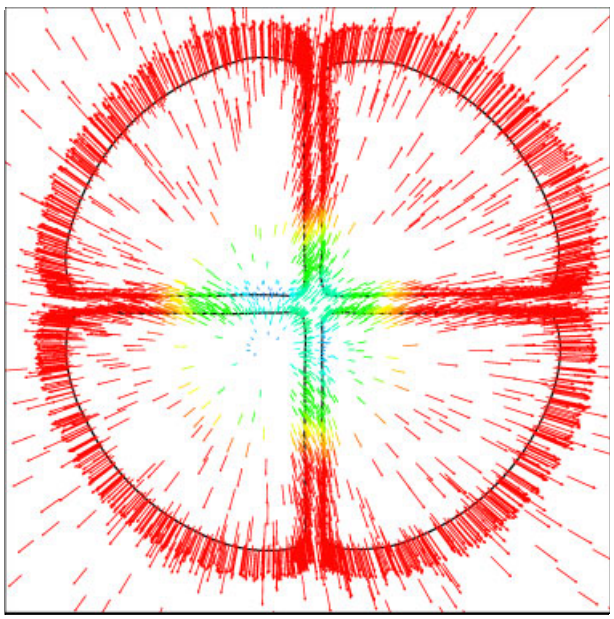

(a)

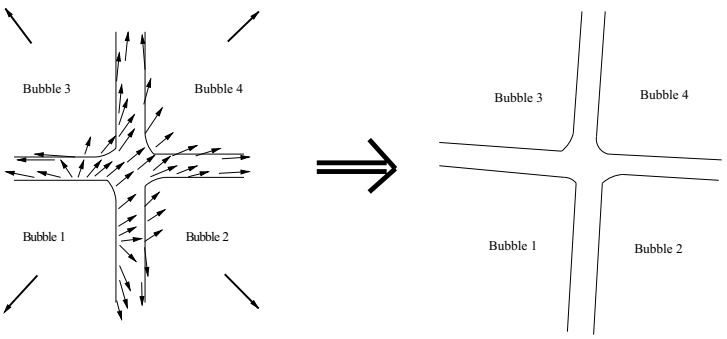

(b)

Figure 17. Expansion of four bubbles: velocity field (first stage of the expansion): (a) $t = 0.75$; and (b) topological rearrangement: rough description of the velocity field at $t = 0.75$ and induced configuration.

expansion. Hence, the velocity field plotted in Figure 10(a) is similar to the one of an expansion without surface tension (see [8]). That can be explained by two factors. The first one is the distance separating the bubble surfaces, which is high enough to limit the effect of a curvature difference. The second factor is the small contribution of the surface tension term (equal to 0.1 at $t = 0$) to the normal stress exerted on the liquid, compared with the one of the gas pressure (equal to 1 at the beginning). However, note that the gas pressure decreases as $1/R^2$, while the surface tension term decreases as $1/R$.

DOI: 10.1002/fld

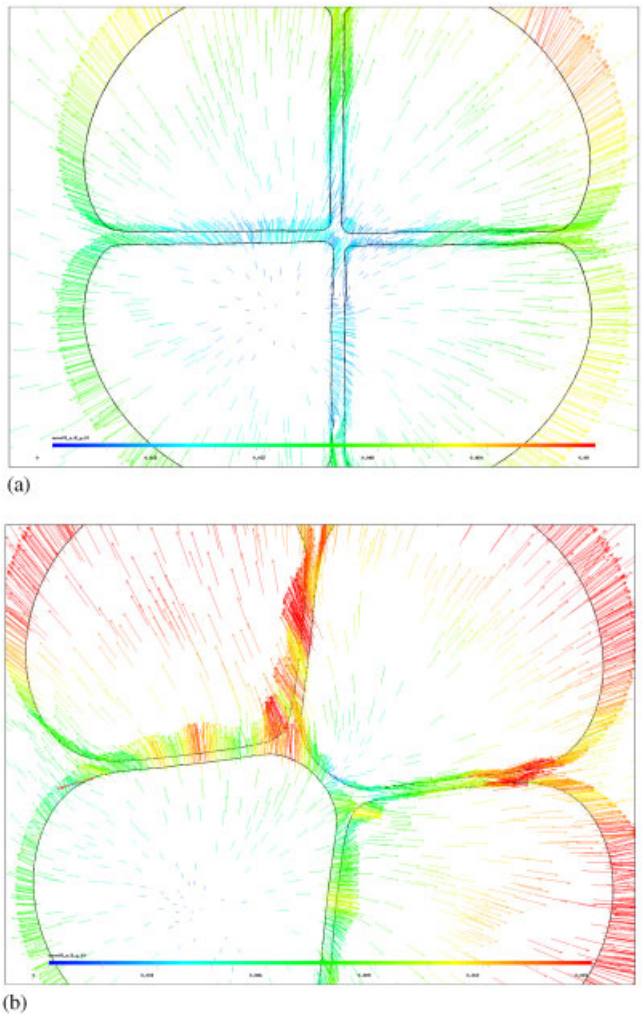

Figure 18. Expansion of four bubbles: velocity field (first and middle stages of the expansion): (a) $t = 7$; and (b) $t = 37$.

During the second stage (Figures 8(c) and (d)), the bubble surfaces are close to each other and the expansion is affected by the surface tension. Hence, during this period, the velocity field (Figures 10(b) and 12(a)) shows a special orientation in the centre of the cluster, due to the differences between the local curvatures. For interpreting this velocity, let us consider Figure 11(a) describing the situation. First, by looking at Figure 13, note that the three bubbles have approximatively the same volume, and then the same inner pressure p_g, all along their expansion. Since $\alpha_1 > \alpha_2$, $1/R_1 < 1/R_2$, the norm $|(p_g - \gamma/R_1)|$ of the normal stress exerted by the bubble 1 on the liquid matrix, is higher than $|p_g - \gamma/R_2|$, the norm of the normal stress induced by the bubble 2. Assuming $\alpha_2 < \alpha_3$ (as in the simulation), Figure 11(b) gives a rough description of the velocity

DOI: 10.1002/fld

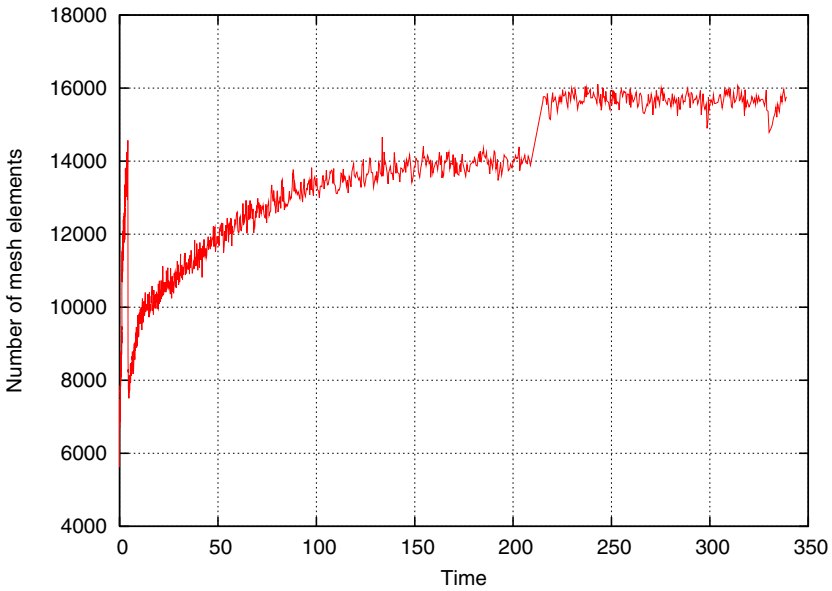

Figure 19. Expansion of four bubbles: evolution of the number of mesh elements.

field resulting from the stress difference: bubble number 2 cannot grow in the direction of bubble numbers 1 and 3. Furthermore, such a velocity field leads to a decrease of α_1 and an increase of α_2: this behaviour is the one observed in Figure 8.

Finally, angles α_1, α_2 and α_3 reach the value of 120°, with a precision of more or less three degrees (Figures 8(e) and (f)). This value appears to be an equilibrium value: since the three bubbles have the same local curvature in the vicinity of the cluster centre, their relative positions do not evolve any more. Because the pressure in the matrix is uniform (and equal to zero in the simulation), a bubble should reach a spherical shape at the equilibrium (Laplace's law). Hence, during the last period, the angles remain unchanged, but the bubbles tend to recover a spherical shape. The bubble volume, plotted over the time in Figure 13 shows that the expansion stops at $t = 600$, approximately. The velocity field has the form considered in Figure 12(b): the expansion is stopped, while small curvature differences provide oscillations of the velocity into the cluster. Note that bubbles of Figure 8(f) have not reached their equilibrium state yet. Their evolution towards the equilibrium proceeds very slowly.

To conclude, the evolution of the number of elements generated by the mesh adaptation is plotted in Figure 14. This number is proportional to the length of the bubble boundary.

4.3. Expansion of a four bubble cluster

This simulation has been performed by considering: $p_{\text{ext}} = 0$, $p^0_{\text{g}_i} |\Omega^0_{\text{g}_i}| = 0.2$ and $|\Omega_{\text{g}_i}| \simeq 0.17$, $i = 1, 2, 3, 4$. The surface tension coefficient is $\gamma = 2 \times 10^{-2}$. The initial configuration, depicted in Figures 15(a) and 17(b) is a pathological one: the bubbles are identical and are forming a group of four meeting at angles of 90°. They are inscribed in a circle of radius 0.5, and spaced by

DOI: 10.1002/fld

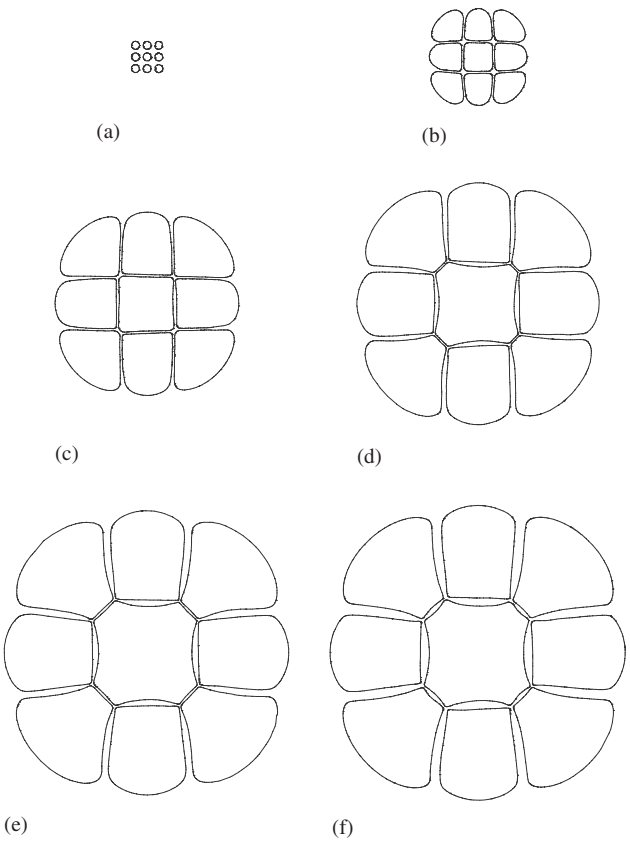

Figure 20. Expansion of nine bubbles: (a) $t = 0$; (b) $t = 47$; (c) $t = 263$; (d) $t = 534$; (e) $t = 800$; and (f) $t = 839$.

a distance of 0.05. As in the previous case, the squared computational domain has a side length of 10. The velocity field is forced to vanish in its four corners.

Figure 15 shows the expansion of the bubble cluster. Due to the closeness of the interfaces in the initial configuration, the topological change depicted in Figure 7(a) occurs as soon as the simulation starts (Figures 15(c) and (d)). The cluster reaches its stable configuration at time $t \simeq 100$, forming two groups of three bubbles meeting at angles of 120°. During this rearrangement, the bubble volumes become heterogeneous, as it can be seen in Figure 16. Beyond $t = 100$, the bubbles continue to grow but remain in this stable configuration. At $t = 200$, the two larger bubbles reach their equilibrium size: their expansion is stopped. The two others evolve progressively towards this same equilibrium size.

The topological rearrangement may be explained by looking at the velocity field. Figure 17 shows that it occurs very soon at the beginning of the simulation. Indeed, at time $t = 0.75$, the velocity field is directed outwards bubble number 1, showing that the local curvature of this bubble is the lowest. Although the four bubbles were considered initially as being identical, numerical

DOI: 10.1002/fld

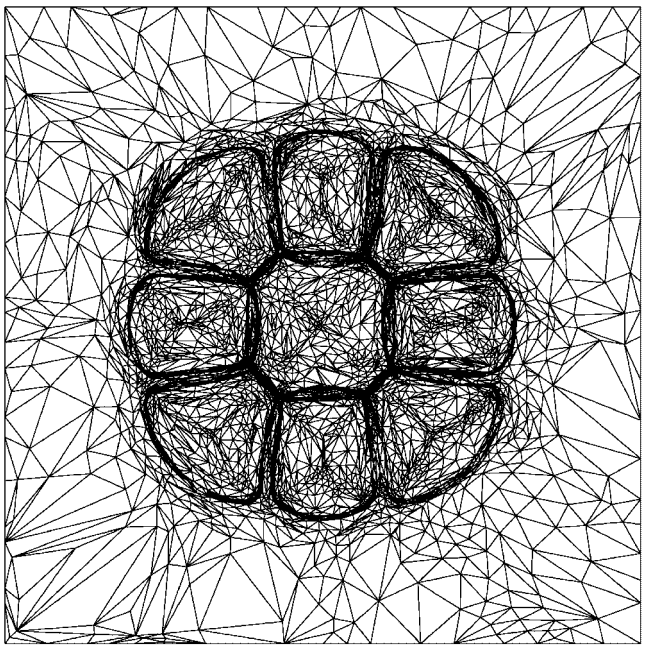

Figure 21. Expansion of nine bubbles: mesh at $t = 839$.

approximations in the construction of the signed distance function provide this observed asymmetry. The configuration resulting from such a velocity field is roughly depicted in Figure 17(b), and corresponds to the expected topological change. The velocity field keeps the same shape during the bubble rearrangement (see Figure 18(a)), until bubble number 2 is far enough from bubble number 3. Then, the velocity field between bubble numbers 1–3 from one side, and between bubbles 2–4 from the other side, is the same as in the three bubble case of Section 4.2, as shown in Figure 18(b).

The number of elements provided by the mesh adaptation is plotted in Figure 19. It follows the evolution of the length of interfaces. The first time steps of the simulation are more difficult from an adaptation standpoint since the mesh has to reach a prescribed accuracy. This explains the first jump in the number of elements. The second jump, at $t \simeq 200$, corresponds to a change in the adaptation parameters.

4.4. Expansion of a nine bubble cluster

Finally, the configuration shown in Figure 20(a) is considered: nine spherical bubbles of radius 0.09 are disposed along a regular grid with a centre-to-centre distance of 0.24. The other parameters are: $p_{\text{ext}} = 0$, $p^0_{g_i} |\Omega^0_{g_i}| = 2\pi \cdot 10^{-2}$ and $\gamma = 10^{-3}$. Furthermore, as in previous cases, the squared computational domain has a side length of 10. The velocity field is enforced to vanish in its four corners.

The evolution of the cluster, obtained by simulation, is shown in Figure 20 at six different steps of its expansion. The final mesh is presented in Figure 21 showing how the mesh and the

DOI: 10.1002/fld

solution are closely related. Topological changes occur and the Plateau's rule is clearly respected: bubbles meet in groups of three, at angles of 120°. These topological changes are similar to the one depicted in Figure 15, except that bubbles have a smaller number of degrees of freedom for moving. For example, the centre bubble cannot have any motion of rotation. Hence, with respect to the angles of 120°, bubble surfaces must be curved as in Figure 20. Since the bubbles of Figure 20(f) are not spherical, the equilibrium state is not yet reached. However, a comparison between Figures 20(e) and (f) shows that bubbles are slowly recovering their spherical shape, leading to an increase in the distance separating their surfaces. The simulation has not been carried out until the equilibrium state is reached, because the process is very slow and its description requires too thin a mesh for the used numerical method (direct method to solve the linear system). Regarding the evolution of the cluster, the expected equilibrium configuration should be similar to the initial one (Figure 20(a)).

5. CONCLUSIONS

A numerical methodology, based on a finite element approach, has been developed for the direct simulation of small bubble clusters. A velocity–pressure mixed formulation has been established over the whole computational domain, by extending to the gaseous part, the velocity and the pressure fields, already defined in the liquid part by Stokes' equations. The liquid–gas coupling has been performed through the gas pressure and the surface tension. The gas pressure is uniform inside each bubble and is related to its volume through an ideal gas law. A level set method, combined with a mesh adaptation technique, has been used to track the interfaces. Since one single distance function has been considered to describe all the bubbles, a special algorithm has been developed to calculate the individual volume of each bubble, which is required for the gas pressure computation.

The expansion of one single bubble has been investigated. Comparisons with an analytical model and with the Laplace's law predictions, have proved the accuracy of the presented approach, especially for the liquid–gas coupling. These comparisons have revealed the importance of the boundary effects, occurring if the computational domain characteristic length is not large enough.

The expansion of small bubble clusters (3, 4 and 9 bubbles) has been successfully simulated. Topological rearrangements occur during the simulations, giving rise to a transient step, in which different bubble sizes may appear. Finally, an equilibrium state is nearly reached, in which only three-bubble groups meeting at angles of 120° are present, as predicted by Plateau's rule.

The presented approach allows to combine both the gas compressibility (involved in an expansion step, for instance) and the minimization of the interfaces, through the action of surface tension. It makes possible the investigation of the bubble cluster evolution far from the equilibrium state, as well as near an equilibrium state, through the description of the bubble shapes, of the velocity field inside the liquid and of the gas pressure.

This work can be improved in many ways. Firstly, by reducing the CPU time of the computations. Actually, the presented simulations take several days, running on a processor Xeon 2, 4 GHz, with meshes of about 7000 nodes. This high CPU time cost limits the bubble number to around 10. On a physical viewpoint, gas diffusion could be investigated in order to have a more realistic expansion step. Taking into account the disjoining pressure could also improve the physics of the simulation, allowing to obtain equilibrium states in which bubbles are not spherical any more.

DOI: 10.1002/fld

REFERENCES

1. Almgren FJ, Taylor JE. The geometry of soap films and soap bubbles. *Scientific American* 1976; **235**:82–93.
2. Weaire D, Hutzler S. *The Physics of Foams*. Oxford: New York, 1999.
3. Weaire D, Cox SJ, Graner F. Uniqueness, stability and Hessian eigenvalues for two-dimensional bubble clusters. *European Physical Journal E* 2002; **7**:123–127.
4. Cox SJ, Vaz MF, Weaire D. Topological changes in a two-dimensional foam cluster. *European Physical Journal E* 2003; **11**:29–35.
5. Vaz MF, Cox SJ, Alonso MD. Minimum energy configurations of small bidisperse bubble clusters. *Journal of Physics*: *Condensed Matter* 2004; **16**:4165–4175.
6. Graner F. *Morphology of Condensed Matter—Physics and Geometry of Spatially Complex Systems*. Springer: Berlin, 2002.
7. Brakke K. The surface evolver. *Experimental Mathematics* 1992; **1**(2):141–165.
8. Bruchon J. Etude de la formation d' une structure de mousse par simulation directe de l' expansion de bulles dans une matrice liquide polymère. *Ph.D. Thesis*, Ecole Nationale Supérieure des Mines de Paris, 2004.
9. Fortin A, Benmoussa K. Numerical simulation of the interaction between fluid drops in multi-phase flows. *Journal of Computational Physics* 2006, submitted for publication.
10. Fortin A, Benmoussa K. An adaptive remeshing strategy for free-surface fluid flow problems. Part I: The axisymmetric case. *Journal of Polymer Engineering* 2006; **26**(1):21–58.
11. Everitt SL, Harlen OG, Wilson HJ, Read DL. Bubble dynamics in viscoelastic fluids with application to reacting and non-reacting polymer foams. *Journal of Non-Newtonian Fluid Mechanics* 2003; **114**:83–107.
12. Kern N, Weaire D, Martin A, Hutzler S, Cox SJ. Two-dimensional viscous froth model for foam dynamics. *Physical Review E* 2004; **70**.
13. Caboussat A, Picasso M, Rappaz J. Numerical simulation of free surface incompressible liquid flows surrounded by compressible gas. *Journal of Computational Physics* 2005; **203**(2):626–649.
14. Brackbill JU, Kothe DB, Zemach C. A continuum method for modeling surface tension. *Journal of Computational Physics* 1992; **100**:335–383.
15. Béliveau A, Fortin A, Demay Y. A two-dimensional numerical method for the deformation of drops with surface tension. *International Journal of Computational Fluid Dynamics* 1998; **10**:225–240.
16. Sethian JA. *Level Sets Methods and Fast Marching Methods*. Cambridge Monograph on Applied and Computational Mathematics, vol. 3. 1986.
17. Brooks AN, Hughes TJR. Streamline upwind/Petrov–Galerkin formulations for convection dominated flows with particular emphasis on the incompressible Navier–Stokes equations. *Computer Methods in Applied Mechanics and Engineering* 1982; **32**:199–259.
18. Sussman M, Fatemi E. An efficient interface preserving level set re-distancing algorithm and its application to interfacial incompressible fluid flow. *SIAM Journal on Scientific Computing* 1999; **20**(4):1165–1191.
19. Belhamadia Y, Fortin A, Chamberland A. Three-dimensional anisotropic mesh adaptation for phase change problems. *Journal of Computational Physics* 2004; **201**(2):753–770.
20. Belhamadia Y, Fortin A, Chamberland E. Mesh adaptation for the solution of the Stefan problem. *Journal of Computational Physics* 2004; **194**(1):233–255.
21. Cox SJ, Weaire D, Vaz MF. The transition from two-dimensional to three-dimensional foam structures. *European Physical Journal E* 2002; **7**:311–315.

DOI: 10.1002/fld